Hindawi
Advances in Civil Engineering
Volume 2023, Article ID 1261643, 17 pages
https://doi.org/10.1155/2023/1261643

Research Article

Microvibration Control of Hybrid Platform for High-Tech Equipment in Buildings Using Brain Emotional Learning-Based Intelligent Controller

Chandrasekhara Tappiti and Tzu-Kang Lin

Department of Civil Engineering, National Yang Ming Chiao Tung University, University Road, Hsinchu 30010, Taiwan

Correspondence should be addressed to Tzu-Kang Lin; tklin@nycu.edu.tw

Received 13 February 2023; Revised 15 July 2023; Accepted 21 August 2023; Published 27 October 2023

Academic Editor: Zhipeng Zhao

In the semiconductor industry, the vulnerability of high-tech facilities installed on platforms to ground excitations induced by nearby traffic is significantly pronounced, primarily due to their small-scale dimensions. Consequently, it is imperative to design a smart control technique by effectively utilizing model-free controllers. Recently, adaptive intelligent control algorithms have emerged as a viable alternative to conventional model-based control algorithms. To address this issue, this study meticulously designed a hybrid platform using the adaptive intelligent controller known as the brain emotional learning-based intelligent controller, along with a Sugano fuzzy inference system to effectively optimize the controller's learning parameters. These learning and intelligent-based algorithms offer notable advantages, including the ability to handle nonlinearity, uncertainty, and training capabilities within the control systems. To assess the effectiveness of the proposed controller in mitigating vibrations induced by traffic on high-tech facilities, a three degree-of-freedom structure is employed along with the hybrid platform. Finally, the performance of the hybrid platform in terms of microvibration control levels is meticulously validated using the Bolt Beranek Newman vibration criteria. Simulation results unequivocally demonstrate that the proposed controller outperforms both an uncontrolled system and a traditional linear quadratic regulator controller in terms of reducing the traffic-induced response of the hybrid platform and second floor, respectively. Through the integration of learning and intelligent-based controllers, the velocity levels of both the hybrid platform and the second floor are reduced to approximately 49.02% and remain well within the acceptable standard criteria curves.

1. Introduction

The high-precision machinery installed on the building floors is considerably affected by natural disasters and even mild ground vibrations due to traffic or high-speed rail operations because of its small dimensions and high sensitivity. For the past three decades, civil and structural engineers have increasingly explored how structures and equipment can be controlled to protect them against natural hazards. Generally, the semiconductor manufacturing industry and high-precision manufacturing firms establish their high-tech facilities on building floors by using passive isolation systems. These systems face challenges in adequately mitigating equipment vibration and achieving sufficient response reduction, primarily due to the absence of stiffness isolation devices and the limitations of passive systems. The utilization of building floors and passive isolation systems falls short in providing effective protection and vibration minimization, thereby posing a significant hurdle for these manufacturing firms. Therefore, it is imperative for the semiconductor industry to prioritize the mitigation of microlevel vibrations to protect their valuable and expensive high-precision equipment housed within the buildings. The present study investigation involves the utilization of hybrid control system that integrates passive mounts and active actuators. This novel approach effectively addresses aforementioned challenges, thereby ensuring the safeguarding of precision equipment.

Two types of smart control techniques can be applied. The first comprises the application of a model-based control algorithm, which uses appropriate mathematical statements and can be applied to both linear and nonlinear control systems. The second comprises the use of a model-free controller, which does not use mathematical models but can resolve various complex dynamic problems and uncertainties [1]. The model-free system identification and smart control of the structures are attractive solutions for control engineers because of the many advantages of model-free control. Additionally, various model-free smart control techniques have been developed by refining the soft computing methods. The development of these control algorithms has been based on the biologically inspired intelligent control models, which replicate the key characteristics of intelligent biological systems [2, 3].

A control schema can be organized during the implementation of a structural system under active or hybrid control; this implementation method ensures that a structure responds in a clear and unambiguous manner. The accuracy and appropriateness of a hybrid or active control system are mostly dependent on the control algorithms that are used; such algorithm require precise and suitable control gains to calculate actuator control forces [4–6]. In the semiconductor industry, optical microscopes, and integrated circuits, the rapid development of high-precision machinery has considerably increased the demand for efficient microvibration control [7, 8]. Thus, the microvibration attenuation of high-tech machinery platforms that are exposed to ground vibrations due to traffic and floor vibrations must be considered. Amiri and Bagheri [9] and Rofooei et al. [10] employed wavelet analysis and nonstationary Kanai–Tajimi spectrum models to generate artificial acceleration time histories and traffic-induced ground motion. Various simulation experiments have been conducted to derive nonstationary traffic driven ground motions [11], and their results indicated that traffic-induced ground motion have a dominant frequency range, which varies depending on the distance between a source and a facility, the nearby soil conditions, and the type of seismic waves that are present. Furthermore, Rao and Sivasubramanian [12] used a fuzzy controller in conjunction with the self-configurable multiobjective particle swarm optimization (PSO) technique to attenuate the response of seismically excited buildings. The proposed controller optimizes both ideal parameters and actuator positions. Chen et al. [13], developed a backpropagation-through-time neural controller (BTTNC) to provide active control for civil engineering structures under dynamic loading conditions. The controller has two types of applications; an emulator network that specifies the dynamic behavior of a structure, and an action network that produces the control forces for training an ideal design system. Their investigation revealed positive results for the proposed neural network controller with respect to the response reduction of a building in San Jose. Xie and Aly [14] developed a smart passive and semiactive vibration control system for wind turbines that are susceptible to mechanical vibrations and multihazard dynamic loading. Additionally, they proposed a clearly defined solution for complex problems relating to the structural control of wind turbines; the solution involved the use of a controller that can reduce the shear and overturning moment of turbines.

By contrast, Lara et al. [15] used a fuzzy controller and an artificial neural network (ANN) controller (i.e., a nonlinear autoregressive exogenous model) to determine the structural control strategy for a two-story building frame. For both of these controllers, the ANN model outperformed other fuzzy controllers by achieving a response reduction of up to 83%. Zabihi-Samani and Ghanooni-Bagha [16] introduced an adjustable cuckoo search wavelet-based fuzzy controller (ACSWBFLC) to reduce the excessive responses of a three-story benchmark building with MR dampers. In their experiments, a discrete wavelet-based transform controller was used to determine the local energy distribution of seismic forces throughout various frequency bands. Their results releveled that the ACSWBFLC was more effective than traditional fuzzy controllers in suppressing the excessive responses of the benchmark building. Azizi et al. [17, 18] explored the effectiveness of optimized fuzzy controllers for seismically agitated tall buildings by applying an enhanced whale optimization algorithm, a hybrid optimization technique (i.e., ant lion optimizer), and the Jaya algorithm. In their numerical findings, the response reductions that they achieved were considerably more effective for a 20-story building than for a 3-story building. In another study, Azizi et al. [19] examined the effectiveness of a multiverse optimizer based enhanced fuzzy controller for suppressing nonlinear structural responses, and they demonstrated that their proposed algorithm could produce competitive results. Marinaki et al. [20] used a multiobjective differential evolution algorithm and genetic algorithm [21] to determine the optimal parameters for a fuzzy controller that was used to suppress the vibration of beams, measured with piezoelectric sensors and actuators and they reported favorable outcomes for the sinusoidal excitation.

In pursuit, Azizi et al. [22] proposed an upgraded gray wolf optimizer (UGWO) that improved the performance of the standard gray wolf optimizer with respect to the seismic control of vibration in nonlinear structures. Their comparisons revealed that the UGWO outperformed other optimizers and resulted in less damage to the benchmark structures. In addition to performing an experimental verification, Lin et al. [23] conducted a feed-forward predictive earthquake energy analysis to determine the characteristics of an earthquake (i.e., whether it exhibited near-fault or far-field ground motion) and to suppress isolated stiffness variable structural responses. Their results indicated that the proposed novel controller can be used for unanticipated far-field and near-fault earthquake excitations. In another study, Lin et al. [24] developed a smart isolation system by employing a leverage-type stiffness-controllable isolation system and a simple fuzzy controller to reduce the near-fault seismic vibration of two-story isolated buildings. Chen and Chien [25] combined a symbiotic organism search algorithm with a multilayer perception model and an autoregressive exogenous

input model to determine the optimal control force produced by a conventional linear quadratic regulator (LQR) controller. A series of numerical simulations involving a 10-story benchmark building revealed that a machine learning (ML) model can be effectively used to emulate the LQR control force without needing the state variables estimated in practical applications. García-Gutiérrez et al. [26] performed fuzzy control optimization for a magnetic levitation system by applying a metaheuristic algorithm, that is, the cuckoo search algorithm. Their comparative numerical results revealed that fuzzy logic control systems can be employed when fuzzy control methods are necessary and that such systems require less computational time than do trial-and-error processes. Zelleke and Matasagar [27] proposed a semiactive control strategy for mitigating the wind response of a 76-story benchmark building; this strategy incorporates the application of an energy-based predictive algorithm and tuned mass dampers. They reported that their proposed algorithm produced more robust results than other algorithms in terms of response reduction while reducing the mechanical energy of the tested building. Furthermore, numerous researchers [28–30] have employed fuzzy controllers to improve the seismic performance of real building structures and tall buildings during wind and earthquake excitations. These researchers have reported that fuzzy controllers outperform traditional controllers for seismic mitigation and that a reasonable tradeoff exists between using a traditional controller and performing quick evaluations to obtain the optimal control force.

Recent literature findings reveal increasing interest in the application of adaptive intelligent controllers in civil structures and smart control systems designed to cope with natural hazards. Panda et al. [31] developed a robust H_∞- based servo-mechanism controller for better control of seismic responses by taking target tracking problems into account. Their findings show that the developed adaptive controller has a significant potential for reducing interstory drift in both SDOF and MDOF systems. In addition, a brain emotional learning-based intelligent controller (BELBIC) controllers, which are a type of adaptive intelligent controllers, have become an extensively discussed topic in the field of neurology and considerable advancements have been achieved in the past 10 years in the field of civil smart structures [32]. In their study, MR dampers were used to reduce the response of a single degree-of-freedom (DOF) structure and a trial-and-error method was employed to determine the controller learning rate parameters required to achieve the optimal control force, but this method requires a considerable amount of calculation time. In other studies, Cesar et al. [33, 34] employed a BELBIC in conjunction with an evolutionary algorithm (i.e., PSO) to reduce the vibration control of noncollocated buildings with a single degree of freedom and three-story buildings with MR dampers. Their simulation results indicated that the proposed controller outperformed the trial-and-error method for both single and three-story buildings, achieving seismic response reductions of up to 60%. The aforementioned literature findings reveal satisfactory results with respect to the seismic attenuation of civil structures with the aid of adaptive intelligent controllers; however, the satisfactory smart control of buildings has yet to be achieved, and no optimally equipped structures with BEL controllers have been reported [34]. Furthermore, most studies have focused on minimizing structural responses to natural hazards, and few have examined the vibrations of high-precision machinery caused by traffic-induced ground motion.

With the objective of achieving adequate response control over passive platforms for high-tech facilities within a building, a BELBIC was developed in the present study. Furthermore, a fuzzy inference system (FIS) was employed that incorporates BEL to tune the weighing parameters of input signals and the learning rates of amygdale (AM) and orbitofrontal cortex (OC) processing units to compensate for each other's inadequacies. With the integration of learning-based controller (i.e., BELBIC) and reasoning-system (i.e., FIS), this investigation accomplishes the optimal controlling system that results in the minimization of microvibration and velocity levels for high-precision machinery. The remainder of the present paper is structured as follows. Section 2 comprehensively describes how the governing equation of motion of a hybrid platform and the corresponding building floor were derived. In Section 3, the input excitations derived from a modified Kanai–Tajimi power spectrum and Bolt Beranek Newman-vibration criteria (BBN-VC) curves are defined for a hybrid platform. Section 4 describes the implementation of the proposed BELBIC and FIS for enhancing the performance of a primary controller. In Section 5, the results of the numerical simulations of the second floor and hybrid platform including their microvibration velocities are discussed, and these results are compared with BBN-VC specifications. Finally, the conclusions are drawn in Section 6.

2. Analytical Model of Hybrid Platform

2.1. Modeling of Building and Hybrid Platform Structure. The performance of the proposed control system was assessed by examining a three-story building and a hybrid platform positioned on the second floor of the building, as illustrated in Figure 1 [35]. Vibrations from nearby machinery, traffic, and other sources pose a significant risk to the machinery, particularly on lower floors. Conversely, higher floors offer a quieter and more stable environment, minimizing the potential disruptions that may impact equipment performance. As a result, the implementation of a hybrid platform on the top floor was considered, which can avoid most of the traffic-induced vibration. These building and hybrid platform were tracked using a hybrid control system (comprising active control and passive mounts with leaf springs) that was influenced by traffic-induced ground motion excitations produced by the Kanai–Tajimi spectrum. The equation of motion of the building coupled with the hybrid platform under the control of the active actuator control system can be obtained through Equation (1) as follows:

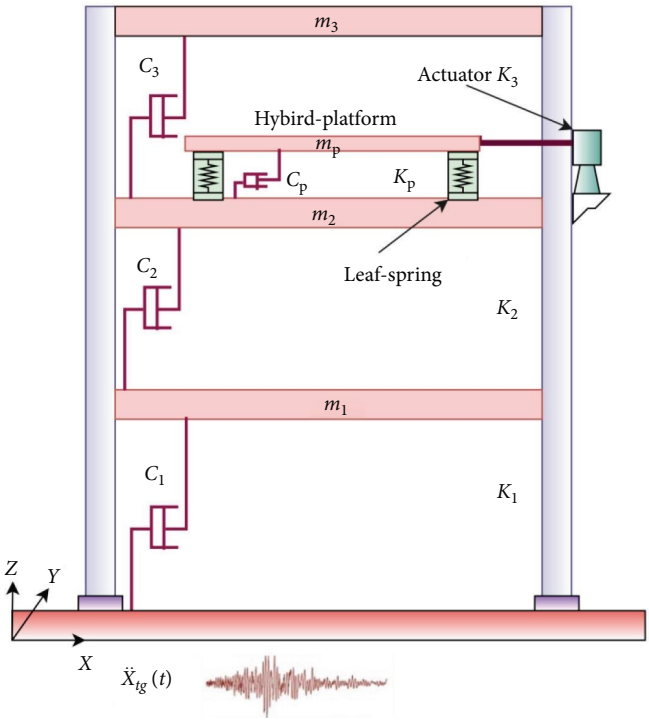

FIGURE 1: Configuration of model building and hybrid platform.

$$\begin{bmatrix} m_1 & 0 & 0 & 0 \\ 0 & m_2 & 0 & 0 \\ 0 & 0 & m_3 & 0 \\ 0 & 0 & 0 & m_p \end{bmatrix} \begin{Bmatrix} \ddot{x}_1 \\ \ddot{x}_2 \\ \ddot{x}_3 \\ \ddot{x}_p \end{Bmatrix} + \begin{bmatrix} c_{11} & c_{12} & c_{13} & 0 \\ c_{21} & c_{22}+c_p & c_{23} & -c_p \\ c_{31} & c_{32} & c_{33} & 0 \\ 0 & -c_p & 0 & c_p \end{bmatrix} \begin{Bmatrix} \dot{x}_1 \\ \dot{x}_2 \\ \dot{x}_3 \\ \dot{x}_p \end{Bmatrix} + \begin{bmatrix} k_{11} & k_{12} & k_{13} & 0 \\ k_{21} & k_{22}+k_p & k_{23} & -k_p \\ k_{31} & k_{32} & k_{33} & 0 \\ 0 & -k_p & 0 & k_p \end{bmatrix} \begin{Bmatrix} x_1 \\ x_2 \\ x_3 \\ x_p \end{Bmatrix} = \begin{Bmatrix} 0 \\ -f_c \\ 0 \\ f_c \end{Bmatrix} + \begin{Bmatrix} m_1 \\ 0 \\ 0 \\ 0 \end{Bmatrix} \ddot{x}_{tg}, \quad (1)$$

where m_i, k_{ij}, and c_{ij} ($i, j = 1$, 2, and 3) are the ith floor's mass, stiffness coefficient, and damping coefficient, respectively; $x_i (i = 1, 2, \text{and } 3)$ is the displacement of the ith floor; $\ddot{x}_{tg}$ is the acceleration of traffic-induced ground motion; m_p, k_p, and c_p are the hybrid platform's mass, stiffness coefficient, and damping coefficient, respectively; x_p, $\dot{x}_p$, and $\ddot{x}_p$ are the hybrid platform's displacement, velocity and acceleration, respectively; and f_c is the control force generated by the BELBIC.

2.2. Equation of Motion in State–Space. The state-space equation of motion of the coupled building and hybrid platform system, derived from Equation (1), is expressed in Equation (2). In regions where heavy traffic-flow vibrations are more likely to occur near the surface or within a specific depth range, it is advisable to concentrate on the first floor when assessing the building's response to traffic-induced ground motion. This approach provides a more accurate representation of the effects of localized vibration sources. By evaluating the state–space model under the influence of traffic-induced ground motion, the responses of the uncontrolled hybrid platform and second floor can be clarified. Focusing on the lower peak ground values of the traffic-induced ground motion and microvibration control scenario, the applied excitation is only considered at lumped mass m_1 as opposed to each mass individually. Application of ground motion at mass m_1 ensures that the structure can withstand the most severe ground motions and provides a conservative estimate of its response performance under the traffic-induced vibration.

$$\{\dot{z}\} = [A]\{z\} + [B] f_c + [E]\, \ddot{x}_{tg}, \quad (2)$$

where $\{z\} = \{x_1 x_2 x_3 x_p \dot{x}_1 \dot{x}_2 \dot{x}_3 \dot{x}_p\}^T$ is the state vector of the coupled building and hybrid platform system; A is the system matrix; B and E are the input matrices for control force and external excitation, expressed as follows:

$$A = \begin{bmatrix} 0 & I \\ -M^{-1}K & -M^{-1}C \end{bmatrix}, B = \begin{bmatrix} 0 \\ B_2 M^{-1} \end{bmatrix}, E = \begin{bmatrix} 0 \\ E_2 M^{-1} \end{bmatrix}, \quad (3)$$

$$B_2 = \{0 - 101\}^T, E_2 = \{1, 000\}^T, \quad (4)$$

where M, K, and C are the building and hybrid platform's collective mass, stiffness, and damping coefficient matrixes, respectively, and B_2 is the placement of the control force. The structural parameters of the building are expressed as follows:

$$[M] = \begin{bmatrix} 100.7 & 0 & 0 & 0 \\ 0 & 100.7 & 0 & 0 \\ 0 & 0 & 100.7 & 0 \\ 0 & 0 & 0 & 20.5 \end{bmatrix} (\text{kg}), \quad (5)$$

$$[C] = \begin{bmatrix} 95.26 & -32.74 & 5.75 & 0 \\ -32.74 & 286.8 & -28.57 & -190.11 \\ 5.75 & -28.57 & 64.37 & 0 \\ 0 & -190.11 & 0 & 190.11 \end{bmatrix} (\text{N s m}^{-1}), \quad (6)$$

$$[K] = \begin{bmatrix} 3.5322 & -1.9364 & 0.2102 & 0 \\ -1.9364 & 3.5201 & -1.8079 & -0.0306 \\ 0.2102 & -1.8079 & 1.6751 & 0 \\ 0 & -0.0306 & 0 & 0.0306 \end{bmatrix} \times 10^6 \ (\mathrm{N\,m^{-1}}). \tag{7}$$

The stiffness and damping matrices of the building can be identified based on the three natural frequencies, normalized model shapes, and model damping ratios of the building without the platform. The hybrid platform's mass was assumed to be 20.5 kg, equal to 25% of the weight of the second floor. Furthermore, the stiffness k_P and damping coefficient c_p of the hybrid platform were obtained as follows: $f_P = \left(k_p/m_p\right)^{1/2}/2\pi$, $\xi_p = c_p/\left(4\pi m_p k_p\right)$, where f_P is the hybrid platform's frequency and ξ_p is its damping ratio.

3. Input Excitation and BBN-Vibration Criteria for Hybrid Platform

3.1. Generation of Traffic-Induced Ground Motion. Although both buildings and human beings are vulnerable to natural hazards like earthquakes, traffic, and rail-induced ground motions can also produce continuous vibrations near buildings and affect the high-precision machinery installed within these buildings. Several factors influence these vibrations, including the proximity of high-tech facilities to traffic, soil characteristics, and traffic density. Ground-borne vibrations, resulting from transient stresses beneath ground, propagate away from the source and can affect buildings and high-tech facilities. High-frequency vibrations tend to possess higher energy but attenuate more quickly compared to low-frequency vibrations [36]. The dominant frequency of ground motion is typically between 4 and 30 Hz [37], and low-frequencies dominate the spectrum at various distances from the vibration source. To address the lack of data in seismic-prone megacities, various studies have generated artificial acceleration time histories for these urban areas. The scarcity of data in this regard hampers the development of dynamic responses for existing structures [38]. Typically, these studies utilize a stationary Gaussian process, employing envelope and shape functions to generate nonstationary acceleration time histories.

The objective of this study is to protect and control high-precision machinery by mitigating the threat of microvibrations, particularly those induced by traffic near industrial areas. The study utilizes the Kanai–Tajimi spectrum, which accurately represents the intermittent and random nature of traffic load, to generate nonstationary accelerations in the frequency range of 4–30 Hz. This spectrum acts as a reference for generating traffic-induced ground motions, incorporating the distinctive characteristics of these vibrations.

Numerous studies have employed nonstationary models of the Kanai–Tajimi spectrum to create nonstationary aspects of acceleration time history because of the simplicity and single dominant frequency of such models [39, 40]. Therefore, the modified Kanai–Tajimi power spectral density function was employed to simulate a stationary acceleration time history in the present study. The function is as follows:

$$S_{xx}^{KT}(\omega) = \frac{\left[1 + 4\xi_{g^1}^2\left(\omega/\omega_{g1}\right)^2\right]\left(\omega/\omega_{g1}\right)^2 U_0^2}{\left\{\left[1 - \left(\omega/\omega_{g1}\right)^2\right]^2 + 4\xi_{g^1}^2\left(\omega/\omega_{g1}\right)^2\right\}} \times \frac{1}{\left\{\left[1 - \left(\omega/\omega_{g2}\right)^2\right]^2 + 4\xi_{g^2}^2\left(\omega/\omega_{g2}\right)^2\right\}}, \tag{8}$$

where ω_{g1}, ω_{g2}, ξ_{g1}, and ξ_{g2} are the parameters of the ground motion which represents the site frequency and damping coefficient and U_0 is the ground acceleration intensity selected to emulate the ground acceleration caused by traffic. When the simulated stationary ground acceleration time history is multiplied by the envelope function, the modulated nonstationary ground acceleration can be obtained as follows Equation (9):

$$\phi(t) = \begin{cases} t^2/t_1^2 0 < t \le t_1 \\ 1 t_1 < t \le t_2 \\ \left(t_f - t_1\right)^2/\left(t_f - t_2\right)^2 t_2 < t \le t_f \end{cases}, \tag{9}$$

where $\phi(t)$ is the envelop function used to obtain the nonstationary form of simulated acceleration, t_f is the total time duration of ground acceleration, which was set to 15 s in the present study. The other parameters in Equations (8) and (9) were set as follows: $\omega_{g1} = 5$ Hz, $\omega_{g2} = 40$ Hz, $\xi_{g1} = 0.58$, $\xi_{g2} = 0.45$, $t_1 = 5$ s, and $t_2 = 10$ s.

Figure 2 presents the simulated traffic-induced ground acceleration time history and the corresponding FAS, with a peak value of 0.05 g. To obtain the displacement and velocity time histories, the acceleration depicted in Figure 2 was integrated twice because these were the input excitations and not accelerations. During the integration phase, the acceleration time history was then processed through a high-pass band filter to eliminate velocity and displacement shifts.

3.2. BBN-Vibration Criteria. The VC curves are widely used and regarded as a benchmark for high-precision facilities in vibration-wired equipment analysis and for constructing structures that can maintain the stability of vibration-wired equipment. The performance of hybrid platforms at the microvibration level can be estimated using the BBN criteria, which have been widely used in the other studies [41], including that conducted by Ungar and Gordan [42]. When the BBN criteria were applied in the present study to assess the microvibration level of complex machinery, the absolute velocity time history was selected as the primary estimation parameter instead of the acceleration and displacement. Therefore, in Figure 3 the BBN criteria are represented as VC curves, and their one-third octave band velocity spectrum values are labeled VC–A through VC–E, where the velocity spectra of the hybrid platform and the building floor are expressed in decibels (dB), referred to as 1 μinch/s.

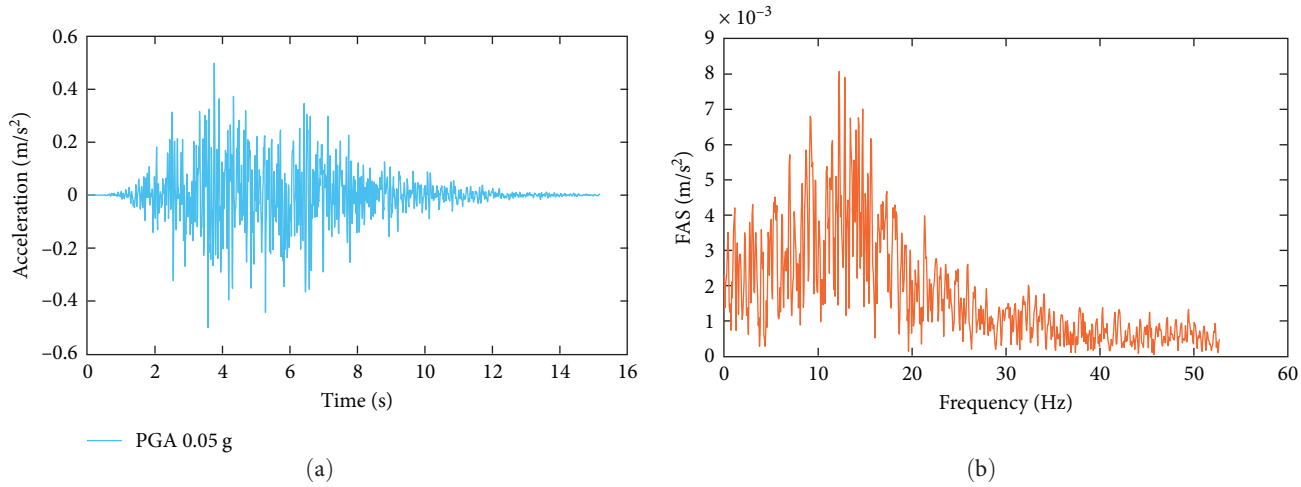

FIGURE 2: Traffic-induced ground motion generated by Kanai–Tajimi spectrum (a) input ground acceleration and (b) Fourier amplitude spectra (FAS).

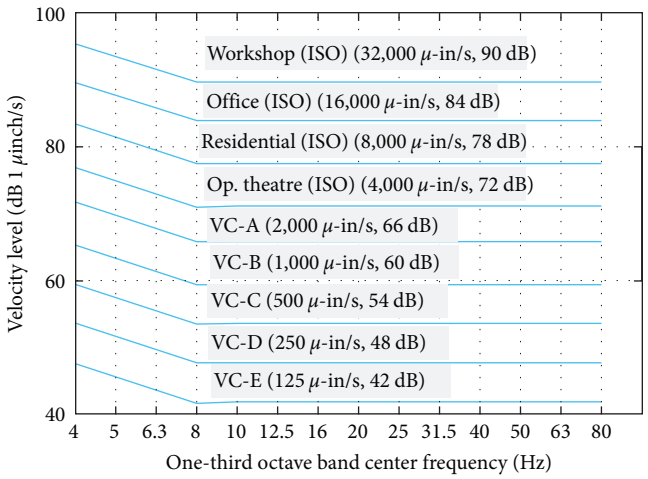

FIGURE 3: BBN-vibration criteria standards for high-precious machinery.

The suggestion from the International Standard Organization regarding how vibrations caused by people in workshops, offices, and other residential structures should be presented were also used as a reference. The most stringent condition of the BBN-VC is that a one-third octave velocity must be less than the VE–E level of 3.12 μm/s (125 μinch/s), and the least stringent VC–A condition is that a velocity that is less than the VC–A level of 50 μm/s (2,000 μinch/s) must have a frequency between 8 and 80 Hz. The present study examined the absolute velocity time histories of the hybrid platform and building floor with and without the use of control devices; these histories were converted to one-third octave band plots to assess the microvibration performance of the control of the hybrid platform. A crucial feature of one-third band filters are that their bandwidth is almost equal to 23% of their center frequency. Given that the one-third octave plots of velocity responses were acquired using the fast Fourier transform (FFT) of these responses (yielding $X(f)$), their approximations were made using the following equation:

$$\dot{X}_{1/3}(n_c) = \left[\sum_{0.89n_c}^{1.12n_c} \left|\dot{X}(n)\right|^2 \Delta n\right]^{\frac{1}{2}}, \tag{10}$$

where $\dot{X}_{1/3}(n_c)$ is the one-third octave band velocity, Δn is the resolution of the FFT, n is the frequency in Hz, and n_c is the center frequency. The aforementioned equation indicates that the one-third octave plots of velocity are constant in the frequency range of 0.89 n_c to 1.12 n_c. In the BBN-VC, the $\dot{X}_{1/3}(n_c)$ is also expressed in decibels referred to $V_0 = 1\,\mu$inch/s, which is expressed as follows:

$$V(n_c) = 20\log_{10}\left[\dot{X}_{1/3}(n_c)/V_0\right], \tag{11}$$

where $V(n_c)$ is the one-third octave band velocity with respect to BBN-VC in dB.

4. Design of BELBIC Control Algorithm

For the analysis of complex and nonlinear dynamic problems, the applications of bioinspired algorithms (e.g., evolutionary algorithms) have increasingly been applied in the various engineering and scientific fields. Notably, the BELBIC proposed by Lucas et al. [43] is a bioinspired technique that is driven and constructed on the basis of the limbic system of the human brain; it was designed to emulate human emotions. The BELBIC has been reported to be a robust tool for investigating problems associated with frequently changing parameters. Moreover, it exhibits other advantages, such as flexibility and the ability to overcome challenges related to performance criteria and uncertainties. The four major components of the BEL system, which is emulating the limbic system, are the AM, OC, thalamus, and sensory cortex (SC). Figure 4 illustrates the key structural blocks and main connections of a controller through the Simulink block diagram proposed by Coelho et al. [44]. Of the components, the thalamus is the first structure to process information from sensory or stimuli input signals. After the preprocessing is completed, the input signals are delivered to the SC and AM units. The SC is responsible for

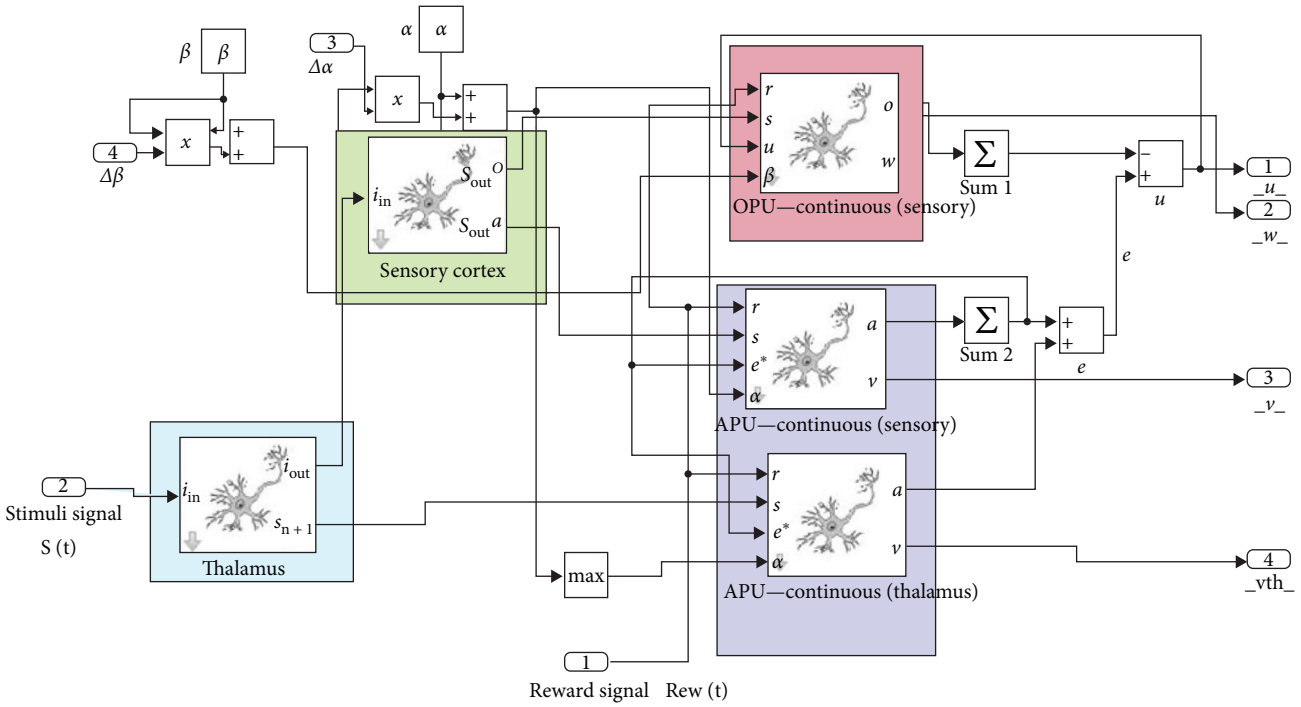

FIGURE 4: Simulink block diagram of BELBIC controller main block.

eliminating the course thalamic output. Subsequently, a filtered signal is transmitted to the AM and OCs. The medial temporal lobe of the brain comprises a small region called the AM, which is responsible for processing the emotional content of input signals, and the OC is a prominent component of the limbic system that inhibits inappropriate amygdala reactions.

On the basis of each DOF, the BELBIC internal processing system can be characterized mathematically as follows [44]:

1. Thalamus: the thalamus functioning as the data transmitter, which transfers the input signal to the SC. The maximum stimuli signal transmitted from the thalamus processing unit to the AM unit is expressed as follows:

$$\mathrm{SI}_{\mathrm{tha}} = \max(\mathrm{SI}_i), \tag{12}$$

where $\mathrm{SI}_{\mathrm{tha}}$ represents the sensory or stimuli input signal from the thalamus processing unit.

2. SC: as depicted in Figure 4, the OC and AM systems receive the thalamus output after the completion of filtering in the thalamus system. Accordingly, the signal does not have any impediments. Because the outputs of the AM and OC system weights can be calculated for every stimuli signal by applying Equations (13)–(16), the output of the main controller, U_i (Equation 16) can be calculated on the basis of the output of the AM and OC processing units.

$$\mathrm{AM}_i = \mathrm{SI}_i V_{\mathrm{AM},i}, \tag{13}$$

$$\mathrm{AM}_{\mathrm{tha}} = \mathrm{SI}_{\mathrm{tha}} V_{\mathrm{tha}}, \tag{14}$$

$$\mathrm{OC}_i = \mathrm{SI}_i W_{\mathrm{OC},i}, \tag{15}$$

$$U_i = \sum \mathrm{AM}_i - \sum(\mathrm{OC}_i + \mathrm{AM}_{\mathrm{tha}}), \tag{16}$$

where AM_i, $\mathrm{AM}_{\mathrm{tha}}$, and OC_i, are the outputs of the AM and OC processing units for ith input; $V_{\mathrm{AM},i}$, V_{tha}, and $W_{\mathrm{OC},i}$ are the weights of the AM and OC units; U_i is the model output.

3. AM and OC units: the primary learning process is completed through the AM and OC units; the learning rates of each unit can be calculated as follows:

$$\Delta V_{\mathrm{tha}} = \alpha_{\mathrm{tha}}(\max[0, SI_i(\mathrm{Rew} - (\textstyle\sum \mathrm{AM}_i))]), \tag{17}$$

$$\Delta V_{\mathrm{AM},i} = \alpha(\max[0, SI_i(\mathrm{Rew} - (\textstyle\sum \mathrm{AM}_i))]), \tag{18}$$

$$\Delta W_{O,i} = \beta(\mathrm{SI}_i(e^* - \mathrm{Rew})), \tag{19}$$

where ΔV_{tha}, $\Delta V_{\mathrm{AM},i}$, and $\Delta W_{O,i}$ are the rate of change of weights in AM and OC processing units and by updating these weights, the learning rates can be calculated; α, and β are the learning rates of the AM and OC processing units, respectively. These rates control the speed at which emotional signals are assimilated into the system output.

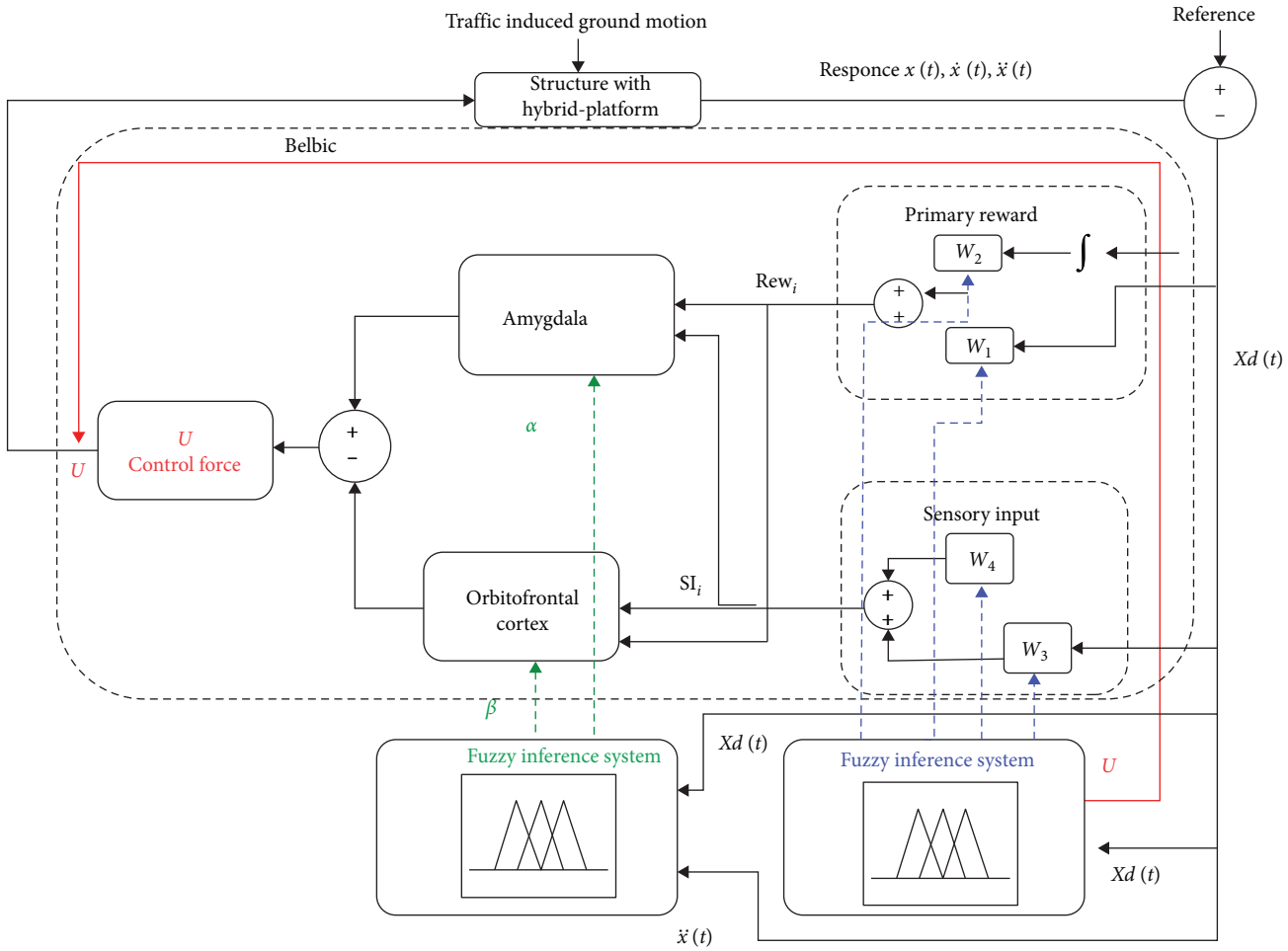

FIGURE 5: Adaptive BELBIC learning process for microvibration control of high-precision machinery.

Furthermore, an output curtailment occurs in the OC unit when the expected signal does not coincide with the reinforcement signal, as demonstrated by Equation (19). The procedure for determining the optimal control force uses the reward or emotional signal (Rew) and stimuli signals, which are typically defined as arbitrary parameters of the input signal and the system output. Another advantage of BELBIC is that it enables researchers to design features that help them to accomplish essential goals. The performance of the BELBIC is solely dependent on the stimuli and reward signals. The relevant equations are as follows:

$$\text{Rew}(t) = \text{Ш}_1 \cdot X_d(t) + \text{Ш}_2 \int_0^t u(t)dt, \tag{20}$$

$$S(t) = \text{Ш}_3 \cdot X_d(t) + \text{Ш}_4, \tag{21}$$

where Rew(t) and $S(t)$ are the reward and stimuli input signals to the BELBIC; Ш_i $(i = 1, 2, 3, 4)$ are the weights that indicate the relative importance of each component, $X_d(t)$ is the relative displacement of each DOF, and $u(t)$ is the anticipated control force or output signal originating from the BELBIC. The incorporation of integral term in the generation of reward signal is commonly acknowledged to enhance the stability of a controller, reduce the steady-state error, and its leads to achieve the superior controller performance [45]. It aids in the reduction of steady-state error by continuously adjusting the control signal, resulting in a smaller error. In addition, it enhances system stability by providing damping and preventing excessive oscillation. Nevertheless, careful parameter tuning is necessary to avoid instability issues. While the current study focused on reducing the displacement and velocity responses, the relative displacement $X_d(t)$ between each floor is taken into the account in the generation of reward and stimuli signals.

With respect to the control algorithm, the optimal control force that could minimize the hybrid platform vibration was obtained using the optimal learning rate parameters of the AM and OC units. Because of the inherent quality of a BELBIC, this type of controller is suitable for the training process but not the reasoning process; therefore, an FIS was used to tune the reasoning knowledge, which includes the associated weights of the Rew(t), and $S(t)$ signals and the learning rate parameters of the AM and OC units. The learning and training process are depicted as a block diagram in Figure 5. The acceleration of the hybrid platform and relative displacement $X_d(t)$ were regarded as inputs to the FIS, which was employed to obtain α and β values. These values play a

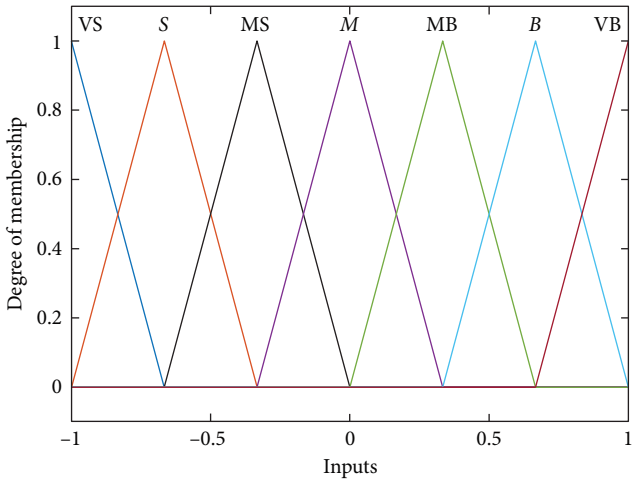

FIGURE 6: Triangular input MFs for the acceleration of hybrid platform and relative displacement.

pivotal role in determining the speed at which the controller learns and updates its internal model based on system inputs and outputs. A higher learning rate enables quick adaptation to system changes, albeit with the potential for instability in certain scenarios. Conversely, a lower learning rate offers more stability but may result in slower adaptation. In the context of vibration attenuation, the learning rate parameters of BELBIC impact the controller's response to vibrations and its ability to adjust control actions for reduction. There is no predefined or fixed set of parameters that can be universally applied. The optimal values for these parameters must be determined through experimentation and tuning, considering the specific dynamics and control objectives of the vibration attenuation system. With the proposed controller, finding an ideal value is flexible and straightforward due to their reward emotional process. Triangular membership functions (MFs) were used for all these input parameters and depicted in Figure 6. However, the rule base of the FIS is presented in Table 1. The subsequent section discusses the results of numerical simulations of the hybrid platform based on the proposed controller.

5. Numerical Simulations and Results

5.1. Linear Quadratic Regulator Controller. The LQR controller is commonly employed in the traditional control domain due to its effectiveness and simplicity of application. According to this technique, the appropriate feedback gain matrix was assessed to achieve a controlled force $f_c(t) = -K_{\mathrm{LQR}} z(t)$, by minimizing the cost function J in the following equation:

$$J = \int_0^\infty \left[z(t)^T Q_{\mathrm{LQR}} z(t) + f_c(t)^T R_{\mathrm{LQR}} f_c(t) \right] \mathrm{d}t, \tag{22}$$

where K_{LQR} is a feedback gain matrix, and Q_{LQR} and R_{LQR} are positive semidefinite matrix and positive scalar vector. It may be emphasized that the optimal solution or gain matrix generated by minimizing the cost function may not be the best solution in all circumstances, due to fact that is determined by the physical constraints of the physical system [46]. In the present work, the obtained values for these matrixes were selected because of better results achieved with their values, as presented in the following equation.

$$Q_{\mathrm{LQR}} = \begin{bmatrix} K & 0 \\ 0 & M \end{bmatrix}, \text{and } R_{\mathrm{LQR}} = 1 \times 10^{-4}. \tag{23}$$

5.2. Comparison of Control Methods with 0.05 g Ground Acceleration. To suppress the vibration within a building caused by traffic-induced ground vibration and that affects the high-precision machinery installed in the building, numerical simulations of a three-story building model and the hybrid platform, which is located on the second floor of the building were conducted. The structural parameters of the hybrid platform and building floors are expressed by Equations (5)–(7) [47]. In ambient vibration, the structure is more sensitive to velocity response as opposed to acceleration response. Considering this, the present study focused on the velocity response-based control as opposed to the acceleration response. Although acceleration remains a crucial metric for vibration analysis, employing velocity response in high-precision machinery vibration control offers a more precise and dependable measurement for ambient vibrations. Furthermore, velocity-based control supplies a more accurate assessment of equipment motion as opposed to acceleration, and this is vital for evaluating the effects of low-frequency vibrations on structural integrity.

To facilitate calculations, the consequence function of the FIS was assumed to be a constant to maximize the efficiency of the controller and the inference system precision. Figure 7 presents the input and output relationship pertaining to a Cartesian rule surface during the process of acquiring the optimal parameters $\alpha \in [0, 1]$ and $\beta \in [0, 0.6]$. The precision of the tested BELBIC was enhanced by selecting the appropriate weights W_i for the input signals such as the stimuli and emotional (reward) signals. These weights were calculated using the method that was applied for the FIS; however, their result function was regarded as constant throughout the inference reasoning process. The values of these modification variables were assumed to within $\mathrm{W}_i \in [0, 6]$. To obtain the associated weights of the input signals for the FIS, two inputs such as the relative displacement $X_d(t)$ between each floor and integral of control force $\int u(t)$ were considered. Each input signal value was distributed using the triangular MFs, and it is depicted in Figure 8 and the rule base is presented in Table 2. The following optimal learning rates for the BELBIC were acquired from the FIS: $\alpha = 0.6667$ and $\beta = 0.0004$.

The proposed controller was designed to protect high-precision machinery from traffic-induced ground vibrations. Therefore, a hybrid platform was considered in this study, and it was designed by the passive mounts and active actuators. In addition, the BELBIC examined in the present study was used to achieve the microvibration control of high-precision machinery positioned on the hybrid platform,

Table 1: FIS rule base for learning rates α and β in the tuning process.

α and β		Acceleration of hybrid platform						
		VS	S	MS	M	MB	B	VB
$X_d(t)$	VS	VB/VS	VB/VS	B/S	B/S	MB/MS	M/M	M/M
	S	VB/VS	VB/VS	B/S	MB/MS	MB/MS	M/M	MS/M
	MS	B/VS	B/S	B/MS	MB/MS	M/M	MS/MB	MS/MB
	M	B/S	B/S	MB/MS	M/M	MS/MB	S/B	S/B
	MB	MB/MS	MB/MS	M/M	MS/MB	MS/MB	S/MB	S/VB
	B	MB/M	MB/MS	MS/MB	S/MB	S/B	S/VB	VS/VB
	VB	M/M	M/M	S/MB	S/B	S/B	VS/VB	VS/VB

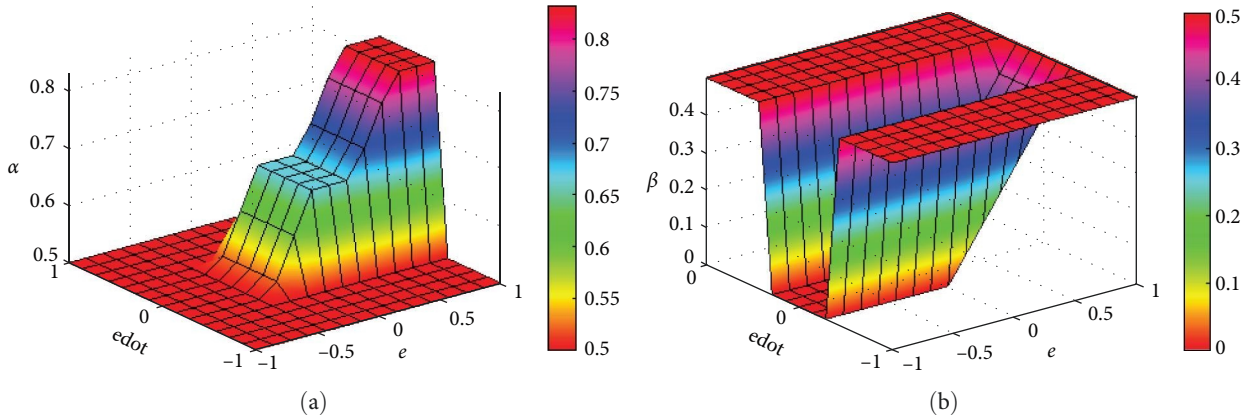

Figure 7: Surface view relations of input and output for learning parameters (a) α and (b) β.

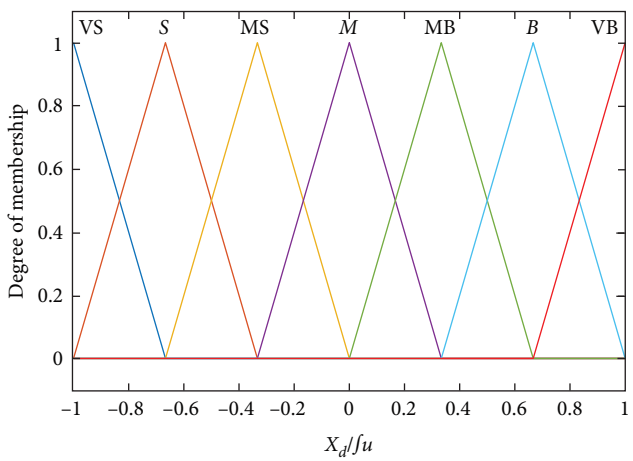

Figure 8: Input MFs of FIS system for $X_d(t)$ and $\int u(t)$.

and the related comprehensive tuning procedure was accomplished with the aid of the FIS. Figure 9 presents the optimized input signal weights in the form of a Cartesian surface, which were acquired from FIS and have the value $\mathbb{W}_i = 3.947$. The results obtained from the BELBIC integrated with the FIS for the second floor and hybrid platform are presented in Figure 10. These results revealed that the displacements of the second floor and hybrid platform were reduced adequately by the LQR controller; however, the velocity response, which was the primary variable indicating the vibration reduction in the present study, was not reduced sufficiently. Consequently, the BELBIC was developed to minimize and maintain the zero-velocity response of the hybrid platform; this was because the high-precision machinery that could be positioned on this table is fragile and highly susceptible to damage from minor vibration. The absolute maximum displacement of the second floor was 1.30, 0.027, and 1.316×10^{-3} mm for the uncontrolled, LQR, and BELBIC scenarios, respectively.

Furthermore, the displacement of the hybrid platform for the uncontrolled, LQR, and BELBIC scenarios, respectively, was 1.20, 0.067, and 4.579×10^{-7} mm. The velocity response of the second floor for the uncontrolled, LQR, and BELBIC scenarios was 110.90, 59.20, and 18.47 mm/s, respectively. However, the comparable absolute velocity of the hybrid platform for these three scenarios was 60.00, 60.21, and 1.80 mm/s, respectively.

The employed controller also achieved an estimated displacement reduction of 90% for both the second floor and the hybrid platform. Similarly, the velocity response was reduced by ~83.34% and 97% for the second floor and hybrid platform, respectively. According to the aforementioned results, the BELBIC controller is noteworthy as it combines emotional learning mechanisms with intelligent control algorithms, enabling it to adapt and learn from the system dynamic behavior. This makes it suitable for handling nonlinearities, uncertainties, and training requirements in semiconductor industry control systems, which is not possible with the LQR controller despite the fact that optimal weights (i.e., Q and R) are known in advance. The maximum

Table 2: FIS rule base for input signals associated weights.

Weights W_i		$\int u(t)$						
		VS	S	MS	M	MB	B	VB
$X_d(t)$	VS	VB/VS/VS/MB	VB/VS/VS/MS	B/S/S/VS	B/S/S/VS	MB/MS/MB/VS	M/M/M/B	M/M/M/MB
	S	VB/VS/VS/MB	VB/VS/VS/MS	B/S/S/VS	MB/MS/MS/S	MB/MS/MS/S	M/M/M/MS	MS/M/M/M
	MS	B/VS/VS/M	B/S/S/MS	B/MS/MS/S	MB/MS/MS/S	M/M/M/MS	MS/MB/MB/MS	MS/MB/MB/M
	M	B/S/S/M	B/S/S/MS	MB/MS/MS/MS	M/M/M/MS	MS/MB/MB/MS	S/B/B/MS	S/B/B/M
	MB	MB/MS/MS/M	MB/MS/MS/M	M/M/M/M	MS/MB/MB/MS	MS/MB/MB/M	S/MB/MB/M	S/VB/VB/M
	B	MB/M/M/VB	MB/MS/MS/MB	MS/MB/MB/MB	S/MB/MB/MB	S/B/B/MB	S/VB/VB/MB	VS/VB/VB/VB
	VB	M/M/M/VB	M/M/M/B	S/MB/MB/B	S/B/B/B	S/B/B/MB	VS/VB/VB/MB	VS/VB/VB/VB

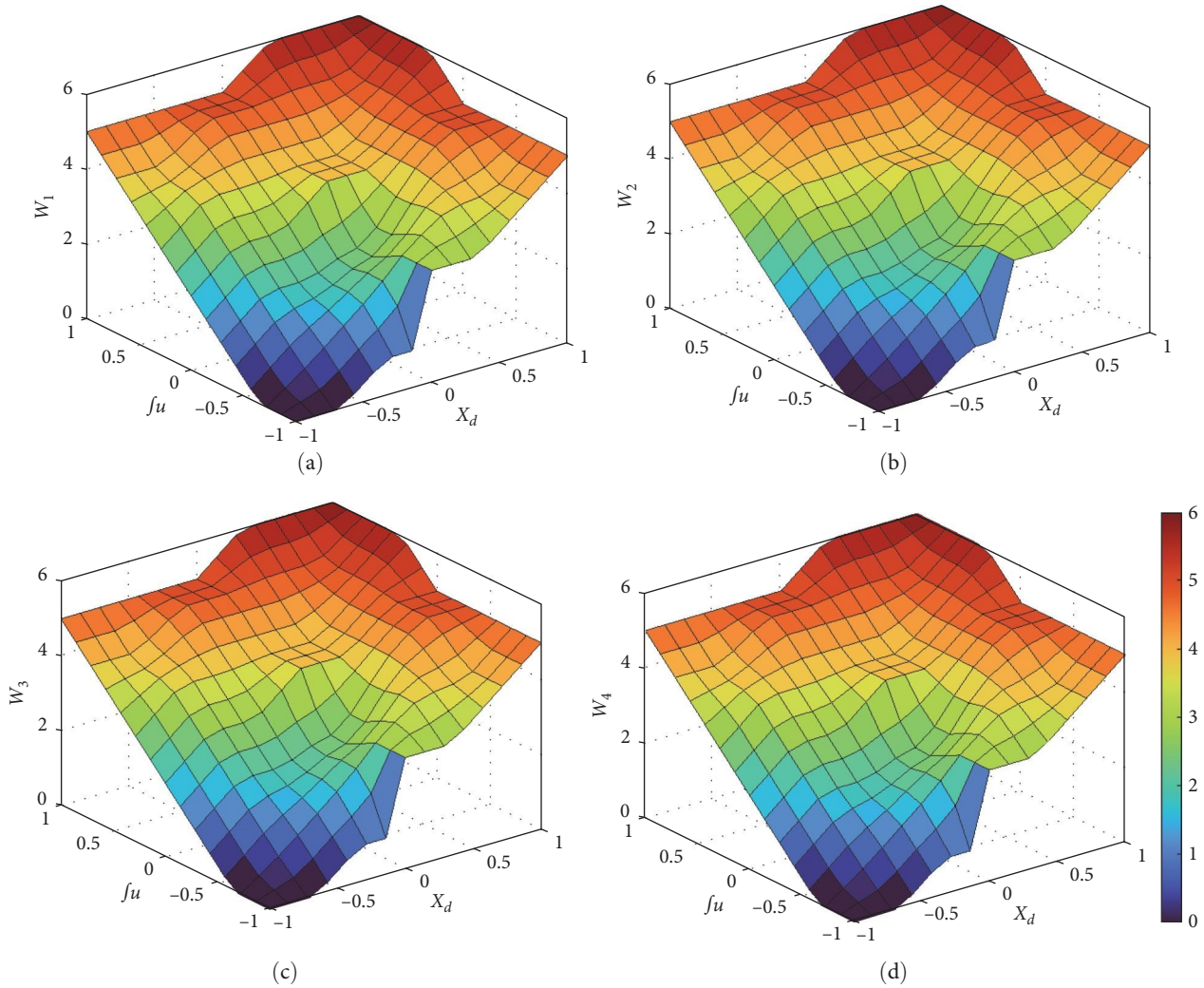

Figure 9: Input and output relations in cartesian surface views for associated weights of BELBIC controller inputs; (a) weight w_1 surface, (b) weight w_2 surface, (c) weight w_3 surface, and (d) weight w_4 surface.

control force delivered to the active actuator, equal to 230 N, was generated by the BELBIC and is illustrated in Figure 11. This was achieved by integrating a fuzzy system to adapt the optimal weighing parameters of the BELBIC input signals. The aforementioned findings indicated that the second floor was affected by the installation of the platform, as evidenced by the nonsignificant increase in the velocity response of the second floor. Therefore, to mitigate the vibration experienced by use of high-precision machinery, the use of hybrid platforms designed with appropriate parameters will not increase response of the floor.

5.3. Comparison of Control Methods with 0.01 g Ground Acceleration. In order to evaluate the performance of the proposed controller, a numerical example with the traffic-induced ground acceleration of 0.01 g was also simulated in

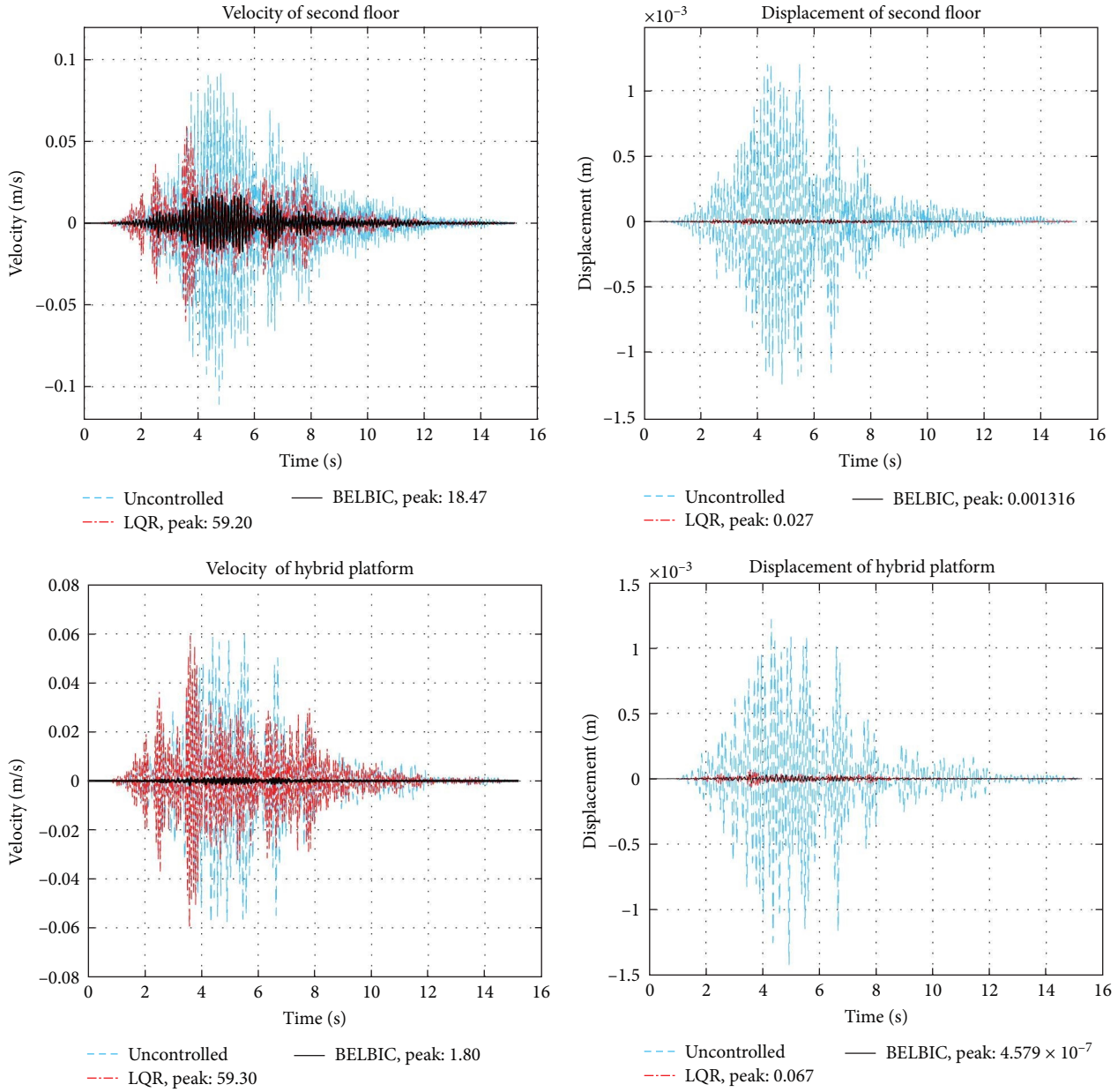

FIGURE 10: Velocity and displacement responses with the PGA of 0.05 g for second floor and platform.

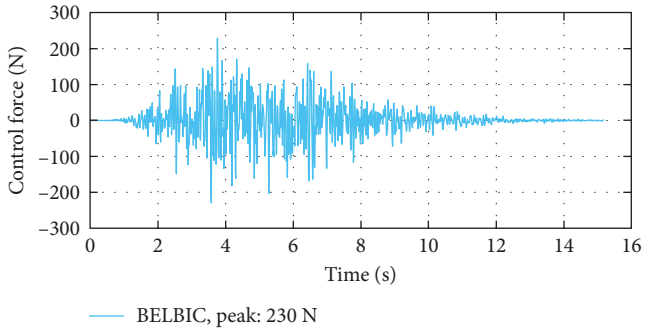

FIGURE 11: The required control force generated by the BELBIC.

this study. The learning rate parameters and input signal weights of the BELBIC controller were assumed to be the same as those used in the aforementioned simulation example with a PGA of 0.05 g. The input signal weighs (Ш_i) were determined as 2.74 for $i = 1$, 2, 3, and 4 using the FIS system. Likewise, the learning rate parameters (α and β) were obtained as 0.56 and 1.242×10^{-7}, respectively. By employing these optimal parameters, the BELBIC controller effectively attenuated the responses of the second floor and hybrid platform without causing any further increase in the floor response. These velocity and displacement responses of the second floor and hybrid platform are presented

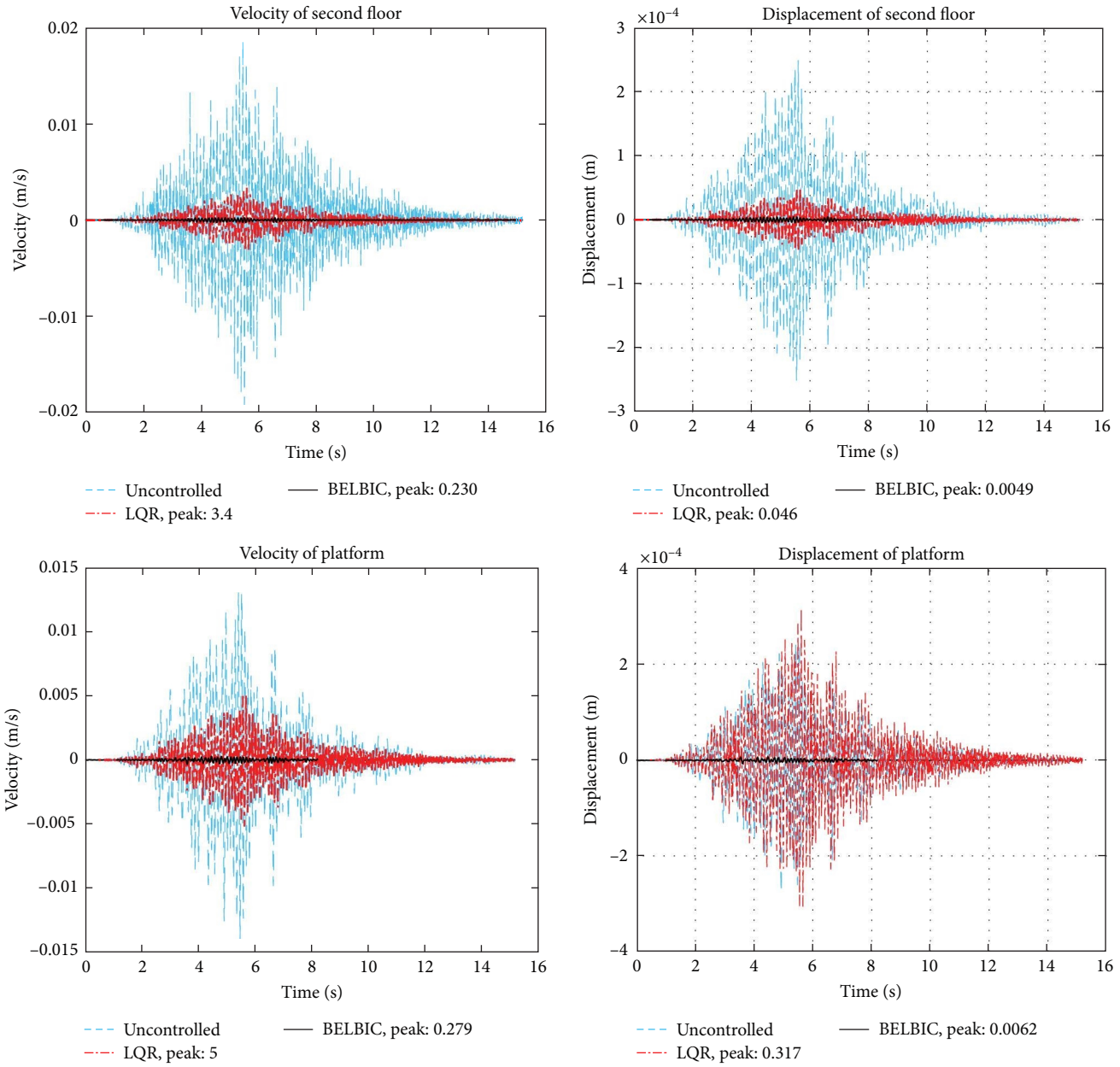

Figure 12: Velocity and displacement responses with the PGA of 0.01 g for second floor and platform.

in Figure 12. According to the result, the maximum absolute displacement of the second floor was 0.25, 0.046, and 0.00449 mm for the uncontrolled, LQR, and BELBIC techniques, respectively. The corresponding displacement of the hybrid platform for the uncontrolled, LQR, and BELBIC techniques, respectively, was 0.27, 0.31, and 0.00623 mm. Similarly, the velocity response of the second floor for the uncontrolled, LQR, and BELBIC techniques was 19.23, 3.4, and 0.230 mm/s, respectively. However, the comparable absolute velocity of the hybrid platform for these three techniques was 13.90, 5.0, and 0.279 mm/s, respectively.

Based on the aforementioned outcomes, the BELBIC controller stands out for its integration of emotional learning mechanisms and intelligent control algorithms. This unique combination empowers the controller to effectively adjust and acquire knowledge from the dynamic behavior of the system as same as 0.05 g simulation example. Consequently, it becomes well-suited for managing nonlinearities, uncertainties, and training demands within control systems in semiconductor industry.

In addition to the mitigation of time history responses, the performance of the proposed BELBIC and velocity levels of the relevant systems were investigated by applying the BBN-VC; this aspect of the present study is discussed in the subsequent subsection.

5.4. Comparison of One-Third Octave Band Spectra. In order to assess the microvibration control performance of the proposed BELBIC technique on a hybrid platform designed to protect high-precision machinery against vibrations caused by traffic, the controlled velocity levels for both the hybrid

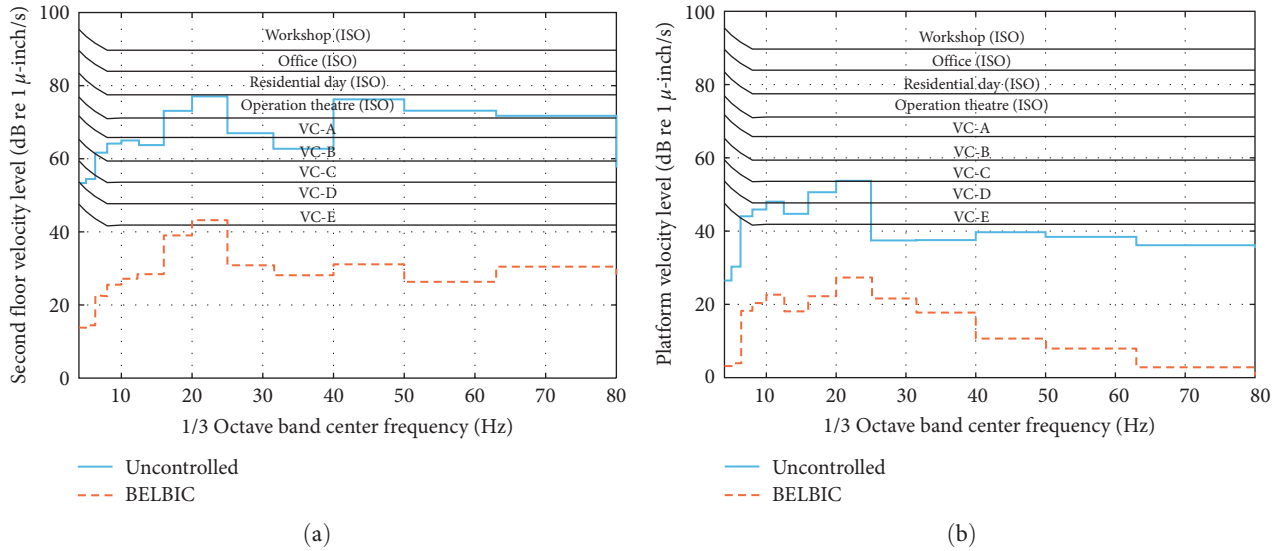

Figure 13: Octave band velocity spectrum of the second floor and hybrid platform for a PGA of 0.05 g. (a) Velocity level of second floor (in dB) and (b) velocity level of hybrid platform (in dB).

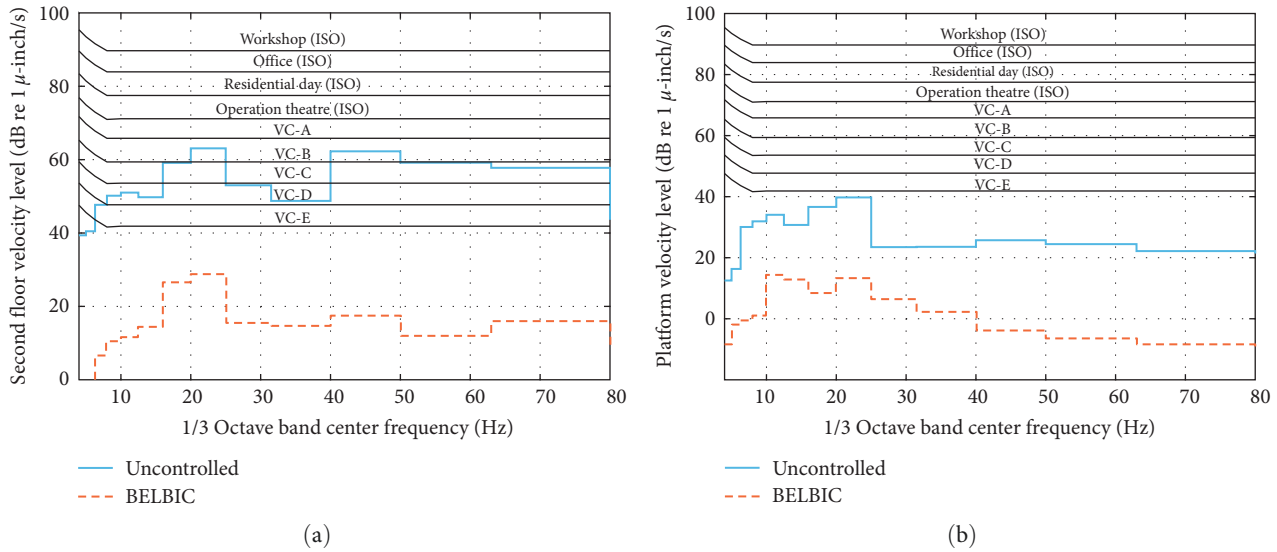

Figure 14: Octave band velocity spectrum of the second floor and hybrid platform for a PGA of 0.01 g. (a) Velocity level of second floor (in dB) and (b) velocity level of hybrid platform (in dB).

platform and the corresponding second floor were measured using the VC curves outlined in Section 3.2. The VC curves were conservative for specific circumstances, particularly for equipment with well-designed integrated vibration control systems. Consequently, the microvibration control performance and velocity levels of high-precision machinery must be assessed on the basis of established standards.

The absolute velocity time histories of the hybrid platform and second floor were converted into a one-third octave plot (velocity spectrum) because the purpose of the study is to design an approach for protecting high-precious equipment. Prior to conducting an assessment of the platform's velocity levels, an evaluation was performed on the velocity spectrum of the second floor to ascertain its suitability for the installation of high-precision machinery.

Subsequently, as illustrated in Figure 13, the velocity spectrum of the second floor and hybrid platform for the proposed BELBIC was then examined under the PGA value of 0.05 g and compared with the BBN-VC specifications. The findings revealed that the maximum velocity level of the second floor in the absence of a control system was 77.49 dB with reference to 1 μinch/s. The velocity level of the second floor exceeds the specified BBN standard threshold and is essential for minimizing the vibration of the floor. Therefore, the BELBIC accounts for the interaction between the building floor and platform to protect high-precision

machinery against floor vibration. When the BELBIC control system was applied, the controlled velocity level of the second floor was 43.19 dB, which was between the values for VC–A and VC–E. Similarly, the velocity level of the hybrid platform with the control system but without a control mechanism was also calculated and depicted in Figure 13(b). The velocity level of the hybrid platform without a control system was 53.59 dB, which also exceeded the standard threshold for high-end manufacturing industries. Thus, velocity levels must be maintained and high-precision machinery must be protected from even small floor vibration. The controlled velocity level of the platform with BELBIC was 27.32 dB, which is below the VC–E curve and meets BBN criteria standards.

Furthermore, the velocity spectrum of both of entities were assessed under PGA value of 0.01 g to check the robustness and performance of the BELBIC; and the results are presented in Figure 14. The examination of numerical example with a ground acceleration of 0.01 g revealed that the BELBIC implementation resulted in velocity levels of 28.78 and 14.12 dB with reference to 1 μinch/s, for the second floor and hybrid platform, respectively. These findings indicated that the proposed BELBIC controller effectively attenuated the velocity level of the high-precision machinery without causing an additional increase in the corresponding second floor's velocity. Additionally, these spectrum values conform to the velocity level specified by the VC–E curves, demonstrating compliance with the BBN-criteria standards. Utilizing BELBIC resulted in notable reduction of one-third octave band velocity level of the hybrid platform, which was lower than the VC curves. Furthermore, this level remained below the threshold VC–E curve.

6. Conclusions

The present study employed a BELBIC algorithm to mitigate the microvibration of high-precision machinery installed in buildings that experience traffic-induced ground motion. This ground motion was generated using the modified Kanai–Tajimi power spectrum because it can represent the characteristics of traffic-induced ground motion. The proposed controller was designed to complete two key tasks, namely, (i) develop a weighing parameter for reward and stimuli signals and (ii) determine the learning rate parameters of AM and OC processing units. These tasks were accomplished by integrating two FISs into the employed controller to empower its performance. To evaluate the performance and robustness of the employed controller, the achieved results are compared to the uncontrolled response and a conventional LQR controller. The conclusive findings of the present investigation are listed as follows:

(i) The present study demonstrated the performance of model-free controllers by coupling two intelligent systems, including fuzzy inference and brain emotional learning, that compensate for each other's inadequacies.

(ii) The acquired results indicated that, compared to the LQR, the BELBIC was more effective in mitigating the responses of the hybrid platform and the second floor of the building investigated. The employed controller also achieved an estimated displacement reduction of 90% for both the second floor and the hybrid platform. Similarly, the velocity response was reduced by approximately 83.34% and 97% for the second floor and hybrid platform, respectively.

(iii) The BBN-VC curves were applied to investigate the effects of BELBIC on the velocity levels of high-precision machinery installed on the designed hybrid platform. When the BELBIC was employed, the one-third octave band velocity level of the hybrid platform was approximately 49.02% lower than the VC curves, which was lower than the threshold VC–E curve.

(iv) In contrast to traditional model-based controllers, the BELBIC is a novel control tool as well as a data-driven controller. Furthermore, in future studies, the BELBIC should be tested under the various ground motion conditions and experimental investigations to clarify its adaptability and robustness in the context of the high-precision machinery manufacturing industry.

Data Availability

The datasets used and/or analyzed during the current study are available from the corresponding author on reasonable request.

Conflicts of Interest

The authors declare that they have no conflicts of interest.

References

[1] M. Bozorgvar and S. M. Zahrai, "Semi-active seismic control of buildings using MR damper and adaptive neural-fuzzy intelligent controller optimized with genetic algorithm," *Journal of Vibration and Control*, vol. 25, no. 2, pp. 273–285, 2019.

[2] B. Blachowski and N. Pnevmatikos, "Neural network based vibration control of seismically excited civil structures," *Periodica Polytechnica Civil Engineering*, vol. 62, no. 3, 2015.

[3] S. Korkmaz, "A review of active structural control: shallenges for engineering informatics," *Computers and Structures*, vol. 89, no. 23-24, pp. 2113–2132, 2011.

[4] Q. Wang, J. Wang, X. Huang, and L. Zhang, "Semiactive non smooth control for building structure with deep learning," *Complexity*, vol. 2017, Article ID 6406179, 8 pages, 2017.

[5] D. H. Zelleke and V. A. Matsagar, "Energy-based predictive algorithm for semi-active tuned mass dampers," *Structural Design of Tall and Special Buildings*, vol. 28, no. 12, 2019.

[6] M. U. Saeed, Z. Sun, and S. Elias, "Research developments in adaptive intelligent vibration control of smart civil structures," *Journal of Low Frequency Noise Vibration and Active Control*, vol. 41, no. 1, pp. 292–329, 2022.

[7] Y. L. Xu, Z. C. Yang, J. Chen, H. J. Liu, and J. Chen, "Microvibration control platform for high technology facilities

subject to traffic-induced ground motion," *Engineering Structures*, vol. 25, no. 8, pp. 1069–1082, 2003.

[8] C.-L. Lee, Y.-P. Wang, and R. K. L. Su, "A study on AGV-induced floor micro-vibration in TFT-LCD high-technology fabs," *Structural Control and Health Monitoring*, vol. 19, no. 3, pp. 451–471, 2012.

[9] G. G. Amiri and A. Bagheri, "Simulation of earthquake records using combination of wavelet analysis and non-stationary Kanai–Tajimi model," *Structural Engineering and Mechanics*, vol. 33, no. 2, pp. 179–191, 2009.

[10] F. R. Rofooei, A. Mobarake, and G. Ahmadi, "Generation of artificial earthquake records with a nonstationary Kanai–Tajimi model," *Engineering Structures*, vol. 23, no. 7, pp. 827–837, 2001.

[11] J. T. Nelson, "Recent developments in ground-borne noise and vibration control," *Journal of Sound and Vibration*, vol. 193, no. 1, pp. 367–376, 1996.

[12] A. Rama Mohan Rao and K. Sivasubramanian, "Multi-objective optimal design of fuzzy logic controller using a self configurable swarm intelligence algorithm," *Computers and Structures*, vol. 86, no. 23-24, pp. 2141–2154, 2008.

[13] H. M. Chen, K. H. Tsai, G. Z. Qi, J. C. S. Yang, and F. Amini, "Neural network for structure control," *Journal of Computing in Civil Engineering*, vol. 9, no. 2, pp. 168–176, 1995.

[14] F. Xie and A. M. Aly, "Structural control and vibration issues in wind turbines: a review," in *Engineering Structures*, vol. 210, Elsevier, 2020.

[15] L. Lara, J. Brito, and C. Graciano, "Structural control strategies based on magnetorheological dampers managed using artificial neural networks and fuzzy logic," *UIS Ingenierías*, vol. 16, no. 2, pp. 227–242, 2017.

[16] M. Zabihi-Samani and M. Ghanooni-Bagha, "Optimal semi-active structural control with a wavelet-based cuckoo-search fuzzy logic controller," *Iranian Journal of Science and Technology, Transactions of Civil Engineering*, vol. 43, no. 4, pp. 619–634, 2019.

[17] M. Azizi, R. G. Ejlali, S. A. Mousavi Ghasemi, and S. Talatahari, "Upgraded whale optimization algorithm for fuzzy logic based vibration control of nonlinear steel structure," *Engineering Structures*, vol. 192, pp. 53–70, 2019.

[18] M. Azizi, S. A. Mousavi Ghasemi, R. G. Ejlali, and S. Talatahari, "Optimum design of fuzzy controller using hybrid ant lion optimizer and Jaya algorithm," *Artificial Intelligence Review*, vol. 53, no. 3, pp. 1553–1584, 2020.

[19] M. Azizi, S. A. M. Ghasemi, R. G. Ejlali, and S. Talatahari, "Optimal tuning of fuzzy parameters for structural motion control using multiverse optimizer," *The Structural Design of Tall and Special Buildings*, vol. 28, no. 13, 2019.

[20] M. Marinaki, Y. Marinakis, and G. E. Stavroulakis, "Fuzzy control optimized by a multi-objective differential evolution algorithm for vibration suppression of smart structures," *Computers & Structures*, vol. 147, pp. 126–137, 2015.

[21] N. Fallah and M. Ebrahimnejad, "Active control of building structures using piezoelectric actuators," *Applied Soft Computing*, vol. 13, no. 1, pp. 449–461, 2013.

[22] M. Azizi, S. Talatahari, and A. Giaralis, "Active vibration control of seismically excited building structures by upgraded grey wolf optimizer," *IEEE Access*, vol. 9, pp. 166658–166673, 2021.

[23] T.-K. Lin, T. Chandrasekhara, Z.-J. Liu, and K.-Y. Chen, "Verification of a stiffness–variable control system with feed-forward predictive earthquake energy analysis," *Sensors*, vol. 21, no. 22, Article ID 7764, 2021.

[24] T.-K. Lin, L.-Y. Lu, and H. Chang, "Fuzzy logic control of a stiffness–adaptable seismic isolation system," *Structural Control and Health Monitoring*, vol. 22, no. 1, pp. 177–195, 2015.

[25] P.-C. Chen and K.-Y. Chien, "Machine-learning based optimal seismic control of structure with active mass damper," *Applied Sciences*, vol. 10, no. 15, Article ID 5342, 2020.

[26] G. García-Gutiérrez, D. Arcos-Aviles, E. V. Carrera et al., "Fuzzy logic controller parameter optimization using meta-heuristic cuckoo search algorithm for a magnetic levitation system," *Applied Sciences*, vol. 9, no. 12, Article ID 2458, 2019.

[27] D. H. Zelleke and V. A. Matsagar, "Semi-active algorithm for energy-based predictive structural control using tuned mass dampers," *Computer-Aided Civil and Infrastructure Engineering*, vol. 34, no. 11, pp. 1010–1025, 2019.

[28] M. M. Javidan and J. Kim, "Fuzzy-based method for efficient seismic performance evaluation of structures with uncertainty," *Computer-Aided Civil and Infrastructure Engineering*, vol. 37, no. 6, pp. 781–802, 2022.

[29] A. S. Ahlawat and A. Ramaswamy, "Multiobjective optimal fuzzy logic controller driven active and hybrid control systems for seismically excited nonlinear buildings," *Journal of Engineering Mechanics*, vol. 130, no. 4, pp. 416–423, 2004.

[30] S. F. Ali and A. Ramaswamy, "Optimal fuzzy logic control for MDOF structural systems using evolutionary algorithms," *Engineering Applications of Artificial Intelligence*, vol. 22, no. 3, pp. 407–419, 2009.

[31] J. Panda, S. Chakraborty, and S. Ray-Chaudhuri, "Development and performance evaluation of a robust suboptimal H∞-based proportional–integral controller–observer system with target tracking for better control of seismic responses," *Structural Control and Health Monitoring*, vol. 29, no. 11, 2022.

[32] M. B. Cesar, J. Goncalves, J. Coelho, and R. C. de Barros, "Brain emotional learning based control of a SDOF structural system with a MR damper," in *Lecture Notes in Electrical Engineering*, pp. 547–557, Springer, 2017.

[33] M. B. Cesar, J. P. Coelho, and J. Gonçalves, "Evolutionary-based BEL controller applied to a magneto-rheological structural system," *Actuators*, vol. 7, no. 2, Article ID 29, 2018.

[34] M. B. Cesar, J. P. Coelho, and J. Gonçalves, "Semi-active vibration control of a non-collocated civil structure using evolutionary-based BELBIC," *Actuators*, vol. 8, no. 2, Article ID 43, 2019.

[35] Y. L. Xu, H. J. Liu, and Z. C. Yang, "Hybrid platform for vibration control of high-precision machinery in buildings subjects to ground motion," *Part 1: Experiment, Earthquake Engineering and Structural Dynamics*, vol. 32, no. 8, pp. 1185–1200, 2003.

[36] T. M. Dawn and C. G. Stanworth, "Ground vibrations from passing trains," *Journal of Sound Vibration*, vol. 66, no. 3, pp. 355–362, 1979.

[37] J. N. Yang and A. K. Agrawal, "Protective systems for high-technology facilities against microvibration and earthquake," *Structural Engineering and Mechanics*, vol. 10, no. 6, pp. 561–575, 2000.

[38] J. A. Abdalla and Y. M. Hag-Elhassan, "Simulation of earthquake ground motion for generation of artificial accelerograms," *WIT Transactions on the Built Environment*, vol. 81, pp. 83–92, 2005.

[39] G. Alotta, M. Di Paola, and A. Pirrotta, "Fractional Tajimi–Kanai model for simulating earthquake ground motion," *Bulletin of Earthquake Engineering*, vol. 12, no. 6, pp. 2495–2506, 2014.

[40] Y. Guo and A. Kareem, "System identification through nonstationary data using time–frequency blind source separation," *Journal of Sound Vibration*, vol. 371, pp. 110–131, 2016.
[41] C. G. Gordon, "Generic vibration criteria for vibration-sensitive equipment," in *Optomechanical Engineering and Vibration Control*, SPIE, 1999.
[42] E. E. Ungar and C. G. Gordon, "Vibration criteria for microelectronics manufacturing equipment," in *Proc. International Conference on Noise Control Engineering*, pp. 487–490, Edinburgh, 1983.
[43] C. Lucas, D. Shahmirzadi, and N. Sheikholeslami, "Introducing BELBIC: brain emotional learning based intelligent controller," *Intelligent Automation and Soft Computing*, vol. 10, no. 1, pp. 11–21, 2004.
[44] J. P. Coelho, T. M. Pinho, J. Boaventura-Cunha, and J. B. de Oliveira, "A new brain emotional learning Simulink toolbox for control systems design," in *IFAC-Papers Online*, vol. 50, pp. 16009–16014, Elsevier, 2017.
[45] J. Panda, S. Chakraborty, and S. Ray-Chaudhuri, "A novel servomechanism based proportional-integral controller with Kalman filter estimator for seismic response control of structures using magneto-rheological dampers," *Structural Control Health Monitoring*, vol. 28, no. 10, 2021.
[46] M. Gopal, *Digital Control and State Variable Methods*, Tata McGraw-Hill, New Delhi, 2nd edition, 2003.
[47] Z. C. Yang, Y. L. Xu, J. Chen, and H. J. Liu, "Hybrid platform for vibration control of high-precision machinery in buildings subject to ground motion. Part 2: Analysis," *Earthquake Engineering and Structural Dynamics*, vol. 32, no. 8, pp. 1201–1215, 2003.